PROCEEDINGS OF SCIENCE

The Rocket Experiment Demonstration of a Soft X-ray Polarimeter (REDSoX)

Herman L. Marshall,[a,*] **Sarah N.T. Heine,**[a] **Alan Garner,**[a] **Rebecca Masterson,**[a] **H. Moritz Günther,**[a] **Ralf K. Heilmann,**[a] **Stephen Bongiorno**[b] **and Eric Gullikson**[c]

[a] *MIT Kavli Institute,*
77 Massachusetts Ave., Cambridge, MA, USA
[b] *NASA Marshall Space Flight Center,*
Huntsville, AL, USA
[c] *Lawrence Berkeley National Laboratory,*
Berkeley, CA, USA

E-mail: hermanm@mit.edu

The Rocket Experiment Demonstration of a Soft X-ray Polarimeter (*REDSoX*) is a NASA-funded sounding rocket instrument that will make the first measurement of the linear X-ray polarization of an astrophysical source in the 0.2-0.4 keV band. We employ multilayer-coated mirrors as Bragg reflectors at the Brewster angle. By matching the dispersion of a dispersive spectrometer using critical-angle transmission gratings to three laterally graded multilayer mirrors (LGMLs), we achieve polarization modulation factors over 90%. We describe the potential science, the instrument, and possible extensions of the design.

Multifrequency Behaviour of High Energy Cosmic Sources XIV (MULTIF2023)
12-17 June 2023
Palermo, Italy

*Speaker

PoS(MULTIF2023)076

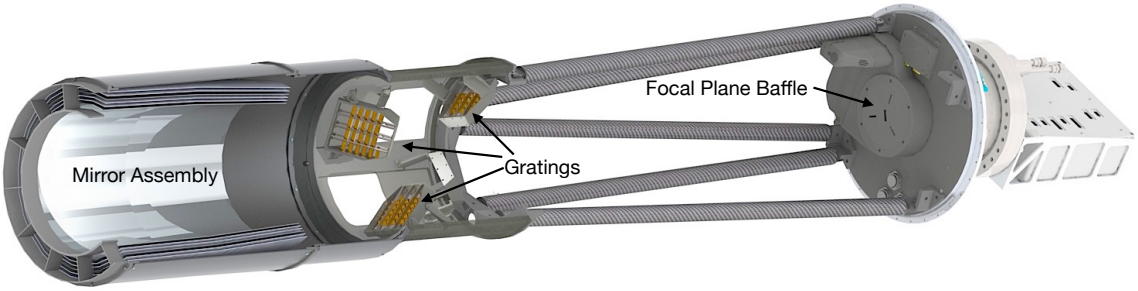

Figure 1: Cutaway rendering of the *REDSoX* Polarimeter from engineering design. The focal plane baffle covers the pendulum valve for the detector chamber. The top and bottom grating groups intercept opposite 60° sectors of focused X-rays, dispersing them through the baffle slit to the left of the central (rectangular) aperture for 0th order. For clarity, only a few mirror shells and grating groups are rendered.

1. Introduction

The first goal of the Rocket Experiment Demonstration of a Soft X-ray Polarimeter (the *REDSoX* Polarimeter,[i] Fig. 1) is to demonstrate the technology needed to measure linear X-ray polarization as a function of energy below 1 keV. The PI and the *REDSoX* team have been working on soft X-ray polarimetry concepts using multilayer-coated optics for over 20 years. Thus, the second goal of this proposal is to pass on the project to early career research scientists, easing them into leadership roles as the project progresses.

This project developed out of earlier, simpler configurations, such as the Polarimeter for Low Energy X-ray Astrophysical Sources (PLEXAS), proposed in 1998 to the low cost NASA "University" Explorer program [41]. That design, copied for the (Chinese) Lightweight Asymmetry and Magnetism Probe [LAMP, 54] and other proposals, was criticized for the limited bandpass of the multilayer coatings – about 5 eV wide – because polarization fractions and position angles vary with energy. The design of *REDSoX* [40, 45] overcomes this weakness by adding laterally graded multilayer mirrors to a grating spectrometer to enable broad-band spectropolarimetry.

We have developed the technology for broad-band soft X-ray polarimetry under the NASA APRA program and are ready for implementation in a sounding rocket experiment. Our baseline design relies on components whose performances have been verified and the design is readily extended to an orbital instrument. We envision that our approach will do for soft X-ray polarimetry what NASA's Imaging X-ray Polarimetry Explorer [*IXPE*, 64, 65] does for 2-8 keV polarimetry. Compared to simple parabolic Bragg reflectors like OSO-8 [63] at 2.6 and 5.2 keV and proposals at 0.25 keV (PLEXAS or LAMP), *IXPE* and *REDSoX* can provide broad-band spectropolarimetry. *IXPE* has sensitivity only above 2 keV, while sources such as isolated neutron stars (NSs) are detectable primarily below 1 keV, where the *REDSoX* design works. The primary target of *REDSoX* is a blazar jet; there are other science goals that would be attainable, either in later flights or with an orbital mission (see § 4.2).

[i]The name of the instrument is used with the permission of Major League Baseball and the Red Sox Baseball Club.

2. Science Objectives

2.1 Probing the Relativistic Jets in BL Lac Objects

While the objective of the *REDSoX* program is to advance technology needed for spectrometers and spectropolarimeters, we also aim to obtain a scientifically valuable measurement. To this end, we have selected the brightest active galaxy as our first target, a "blazar."

Blazars, which include BL Lac objects, high polarization quasars, and optically violent variables, contain parsec-scale jets with $\beta \equiv v/c \sim 0.995$ or higher. In the so-called high-synchrotron-peak blazars (HBLs such as Mrk 421 & Mrk 501), the X-ray spectrum is steeper than the optical spectrum, indicating that the X-rays are produced by synchrotron radiation from the highest energy electrons that are efficiently accelerated close to the base of the jet or at shock fronts farther downstream in the jet. See Fig. 2 for examples of spectral energy distributions of blazars.

For a differential electron energy distribution $n(E) \propto E^{-p}$, the maximum fractional polarization for synchrotron emission from relativistic electrons in a uniform B field is $P_{\rm max} = \frac{p+1}{p+7/3}$ [15]. The spectral shape is a power law with photon index $\Gamma = (p+1)/2$, so $P_{\rm max} = \Gamma/(\Gamma + 2/3)$. For Mrk 421, Γ is typically about 2.5 in the soft X-ray band, giving $P_{\rm max} = 0.79$, i.e., 79% polarized. If the soft X-ray polarization is much less than 79%, then models with simple, uniformly magnetized X-ray emission regions will be ruled out. Recently, *IXPE* has been used to demonstrate that the X-ray emission for some blazars is likely due to synchrotron radiation in stratified shocks in jets [10, 36]. In this model, the polarization in the soft band should be somewhat smaller than that observed above 2 keV, which is 10-20%.

Turbulence causes both the degree and position angle of the polarization to vary erratically about some systemic value. (The electric vector position angle, often denoted EVPA, is usually defined as the angle to the east from north.) In the shock model, the emitting volume decreases with frequency as $\nu^{-1/2}$ because the emitting electrons lose energy as they advect from the shock front where they are energized. The number of emitting turbulent cells, N, then drops to higher frequencies as $\nu^{-1/2}$ and the average polarization $\langle P \rangle = P_{\rm max} N^{-1/2}$ [39], so $\langle P \rangle \propto \nu^{-1/4}$. Thus, in this model the X-ray polarization at 0.3 keV is 3.7 times that in the R-band, giving polarizations of about 20% and 40% for Mrk 421 and Mrk 501, respectively. Furthermore, the EVPA would not likely align with the R-band EVPA as different cells would dominate the two bands. In this model, the polarization in the *IXPE* band should be about 2× larger while a single zone shock model indicates that P should be nearly independent of energy in the X-ray band [59], so comparing *IXPE* and *REDSoX* measurements would test these models. We only have limits to the time scales for polarization variability at present because significant detections with *IXPE* requires exposures of $\sim 10^5$ s. Variability of the EVPA on a scale of minutes or hours would reduce the polarization signal in a daylong observation but the *REDSoX* observation would last only five minutes. Thus, polarization in the *REDSoX* data that is significantly higher than found in *IXPE* data would support the turbulence model.

Both Mrk 421 and Mrk 501 are variable; Mrk 421 is brighter at present, so it is our primary target. We take the median count rate of Mrk 421 from the Swift XRT over the past 10 years as a baseline: 28.5 cnt/s. About 20% of the time, the count rate is ×2 higher. Converting to a spectral flux density using $\Gamma = 2.5$ gives an average of $I = 0.023$ ph cm^{-2} s^{-1} Å^{-1} in the 0.2-0.4 keV band. For the *REDSoX* Polarimeter, the expected minimum detectable polarization (MDP) is 18%. Thus,

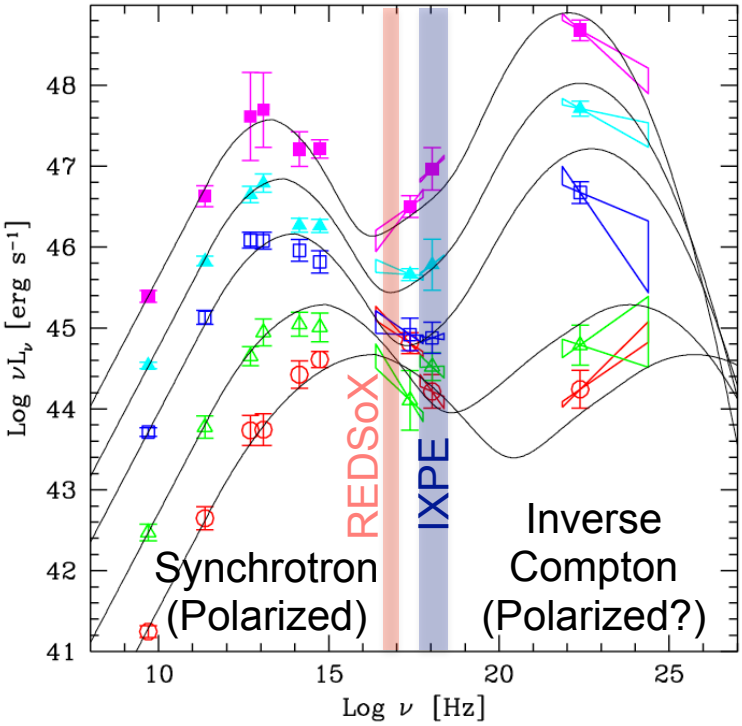

Figure 2: Spectral energy distributions for blazars, showing the blazar sequence where the spectral peak of the synchrotron component inversely correlates to the power in that component (adapted from [11]). The high energy component is considered to be due to Compton scattering of ambient photons off of high energy electrons in the jet and may be polarized in some models. The *REDSoX* bandpass is lower than that of *IXPE*, so it can sample the synchrotron component in "intermediate" blazars that can dominate at soft X-rays while the Compton component dominates in the hard band that *IXPE* samples.

even an upper limit would provide a test of the turbulence model and require that the emission region's B-field be significantly disordered. Mrk 501, as an alternative, is fainter but the predicted polarization is higher. A decision about which target to observe can be made closer to launch, based on monitoring observations.

2.2 Other Targets for a Soft X-ray Spectropolarimeter

REDSoX is the technology leader for an orbital mission (§4.2), so here we describe science from observations of other targets. In addition to Mrk 501, some of these targets can be observed in a reflight of *REDSoX* or of an upgraded version (see §4.2).

2.2.1 Magnetized Atmospheres of Neutron Stars (NSs) and Pulsars

Some of the strongest magnetic fields in the universe are observed in isolated NSs, making them unique laboratories for the interaction of matter and fields, as well as for testing quantum electrodynamics (QED) effects [21]. One of the brightest pulsars in the soft X-ray band is Her X-1, for which *REDSoX* could reach an MDP of 25%. Her X-1 is a pulsar with $B \sim 10^{12}$ G. The nature of the soft X-ray emission is not well understood. The sub-keV pulsed emission of Her X-1 does not come from the surface or polar cap, as its effective size is much larger than the NS, and is more

likely from the inner edge of the warped, highly inclined accretion disk where the magnetosphere disrupts it [29]. While the X-ray emission might be thermal, it is highly pulsed. If the sweeping magnetic field heats the ionized disk and the radiation is predominantly synchrotron, then the soft X-rays would be up to 70% polarized if the field is very ordered there. An upper limit would favor reflection of the beam off of the accretion disk, making it an excellent target for a *REDSoX* reflight.

With soft X-ray spectropolarimetry of isolated NSs, we can understand the origin of atmospheric absorption lines, verify QED predictions, test atmosphere models, and assess effects in pulsar magnetospheres. Atmosphere modeling currently includes linear polarization but this aspect of the models cannot be tested currently. These models are needed in order to accurately determine a NS radius, R, that is key to testing equations of state of matter at nuclear densities [21, 30, 57]. A soft X-ray polarimeter will provide the missing polarimetry information needed to test these atmosphere models (see Fig. 3). *IXPE* will observe NSs to examine magnetospheric phenomena and the effects of QED on the pulsed radiation but the NS surfaces are observable only below 1 keV, which makes these measurements impossible for *IXPE* but perfect for an orbital version of *REDSoX* (§4.2).

Identifying an atmospheric absorption feature by observing the polarization across the feature would provide the gravitational redshift at the NS surface, $z = (1 - 2GM/[Rc^2])^{-1/2} - 1$, giving the NS mass M when R is determined from atmosphere fitting. Measuring z this way has never been done for any NS (although claimed [8] but not confirmed [9]), providing a ground-breaking opportunity. Determining both M and R for any NS is critical for studying the fundamental nature of matter itself. *NICER* has been used for measuring M and R using NS hot spots [4, 5], a method that is difficult to apply to isolated NSs with low pulse fractions. Several such sources have absorption features in their phase-averaged 0.25-0.5 keV spectra that are thought to arise from proton cyclotron features when $B \gtrsim 10^{13}$ G [e.g. 6, 19, 20] or gravitationally redshifted O VIII [31]. The centroid of a deep absorption feature in RX J1308.6+2127 varied with pulse phase, perhaps due to a multipolar magnetic field [6]. As the lines appear to be resolved with FWHM of $\sim$ 150 eV level [6, 20], we require a spectral resolution of better than 50 eV in order to measure the polarization change through the line, as predicted in atmosphere models (Fig. 3 left; [57, 58]). To resolve these lines requires obtaining MDPs of at least 30% in 4-10 bands, feasible for an orbital version of *REDSoX* (see Fig. 3 center and §4.2).

Even without absorption features, the polarization fraction and EVPA vary with energy within the soft X-ray band in a manner that depends on the atmosphere's composition and whether the atmosphere is gaseous or solid (Fig. 3 right, [51]). At these high magnetic fields, the vacuum is birefringent [27, 28], polarizing the X-rays from the surface up to 80% [60] for a gaseous atmosphere but is likely <10% for a condensed surface [66]. Thus, a limit below 50% will likely rule out a gaseous atmosphere. This discrimination capability requires a soft X-ray measurement and cannot be settled with optical polarimetry [66].

2.2.2 Polarization in Disks and Jets of Active Galaxies and X-ray Binaries

Other targets for *REDSoX* or an orbiting soft X-ray spectropolarimeter (§ 4.2) are quasars and X-ray binaries (XRBs). X-ray emission from accretion onto black holes may arise from Compton scattering of thermal photons in a hot corona or from synchrotron emission or Comptonization by electrons in a highly relativistic pc-scale jet. Jets are frequently observed from such sources, so the

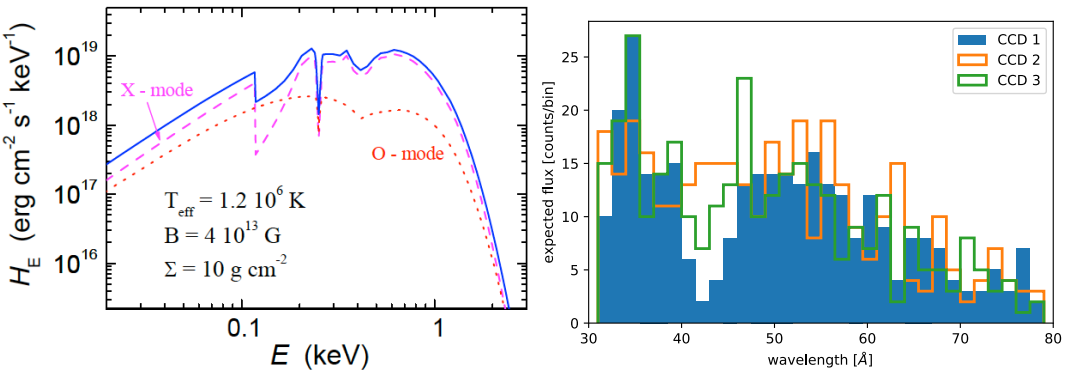

Figure 3: *Left:* Model of an atmosphere showing how the absorption lines appear differently in different polarizations, given by the extraordinary (X) and ordinary (O) modes of photon propagation relative to the local magnetic field [57]. The spectral features show up most prominently in the X mode and would be discernible with a spectropolarimeter with moderate spectral resolution. Such sources are ideal for observations by an instrument such as *REDSoX* with sensitivity below 1 keV but would be nearly impossible to observe with *IXPE*. *Right:* Simulation of a NS atmosphere observed with *GOSoX*, showing each CCD's count spectra. The atmosphere is unpolarized except in an absorption feature at 47Å (260 eV) that is 5 Å (30 eV) wide with an equivalent width of 2.5 Å (15 eV) and 50% polarized along a position angle that nulls the flux in CCD1. Even though there are a total of only 1000 counts, giving a broad-band MDP of 14%, the 50% polarized absorption feature is detectable because *REDSoX* is a spectropolarimeter.

X-rays should be polarized. In both cases, the origin of the jet is not resolved in the X-ray band, so X-ray polarization measurements can give an indication of the existence and orientation of jets within 10^3 gravitational radii.

Transient XRBs with stellar-mass black holes like XTE J1118+480 can be very soft and jets may contribute most of the X-rays [38] – confirmable using polarimetry. A jet model for XTE J1118 indicates that the soft X-ray polarization should be about 20% [62]. The source was discovered with XTE and detected by the Extreme Ultraviolet Explorer at 100 eV, so the column density is well below 10^{20} cm^{-2}. During its 2000 outburst, the flux density at 0.3 keV was brighter than Mrk 421 [47], making it, or an XRB like it, an excellent candidate for a *REDSoX* reflight or a target of opportunity for an orbital mission.

The accretion disks of radio quiet AGN should be ~10% polarized [48, 53] and the polarization angle and magnitude should change with energy in a way that depends on the system inclination. Except for a Compton-thick AGN (Circinus Galaxy, [61]), the best detection of a radio quiet AGN with *IXPE* was in the observation of NGC 4151, which was found to be about 5% polarized [14]. The variation of polarization with energy could be used as a probe of the black hole spin and the EVPA should rotate through 90° between 1 and 2 keV [53]. Thus X-ray polarization measurements are needed both above 2 keV (with *IXPE*) and below 1 keV with a future mission based on the *REDSoX* design (such as *GOSoX*, see §4.2).

3. Instrument Overview

Our project leverages previous funding from flight projects and NASA development grants to make focusing optics, multilayers, gratings, and CCDs. Together, these technologies enable

us to build the *REDSoX* Polarimeter a sensitive X-ray instrument operating in the 0.2 - 0.4 keV energy range, designed to fit a Terrier MK70 Black Brant MK1 sounding rocket. The science payload consists of the X-ray optics with Wolter type I mirror shells, 200 nm period Critical Angle Transmission (CAT) gratings mounted on a 2.5 meter focal length optical bench, the focal plane with four X-ray detectors and three multi-layer mirrors in a high vacuum chamber that is open only while the instrument is over 120 km altitude. See Fig. 1 for an engineering rendering and Marshall et al. [45] for raytrace illustrations of operation.

The basic design [45] involves matching the dispersion of the gratings to the lateral grading of a multilayer (ML) coated mirror set at about 45° to the incoming light. In the X-ray band, this is the Brewster angle, where the reflected light is 100% polarized with the electric vector perpendicular to the reflection plane. CCD detectors view each ML mirror to determine the intensity reflected from that ML mirror. By orienting three ML coated mirrors at position angles 120° apart, we can measure the three Stokes parameters I, Q, and U at any time without instrument rotation. The linear polarization fraction is given by $\Pi = \sqrt{Q^2 + U^2}/I$. The 0th order CCD detector, which is otherwise necessary to confirm telescope pointing, also can be used to determine I, providing some redundancy.

3.1 Focusing Optics

The polarimeter optics proposed here will be fabricated using an electroformed replication process. In this, nickel alloy mirror shells are electroformed on super-polished and figured aluminum mandrels from which they are later separated. The resulting full-shell optics are stable, durable, and have good angular resolution [52]. The procedures for mandrel fabrication, shell replication, and mirror assembly are nearly identical those involved in the *IXPE* mirror fabrication.

For this project, we take advantage of existing technology and equipment at the Marshall Space Flight Center (MSFC). We will use 5 existing mirror mandrels that were fabricated for the Micro-X sounding rocket program (mission 36.245) [37], developed at a cost of ~$1M and replicate mirror shells from them. A mandrel is shown in Fig. 4 (left). For a future version of *REDSoX*, we would have 4 new mandrels fabricated by MSFC. The 4 extra shells add 40% to the effective area of the mirror assembly but would not be fabricated for this program in order to reduce costs. Each shell follows a Wolter 1 prescription with a total length (paraboloid + hyperboloid) of 600 mm and a thickness of 1 mm.

The focal length is 2500 mm, giving a focal plane plate scale of 82″/mm. The mirror module will have a half-power diameter (HPD) of $\lesssim$30″ [16, 52]. The similar *IXPE* optics have HPDs of $< 25''$. Raytracing shows that the system effective area is reduced only 6% if the HPD is as large as 60″, so the system is robust to possible mirror assembly issues. As with other grating spectrometer designs, we will subaperture the mirror (Fig. 4), placing grating modules behind ±30° sectors on opposite sides of the focusing light path to reduce the telescope 2D PSF from 30″ to 10″ in 1D [45] for use in spectroscopy [7], projecting to $\delta x = 120\mu$m along the dispersion.

3.2 Gratings

We use Critical-Angle Transmission (CAT) gratings [23] developed in the Space Nanotechnology Lab (SNL) at MIT that can now be reliably produced in a 10×30 mm format [22, 24]. By

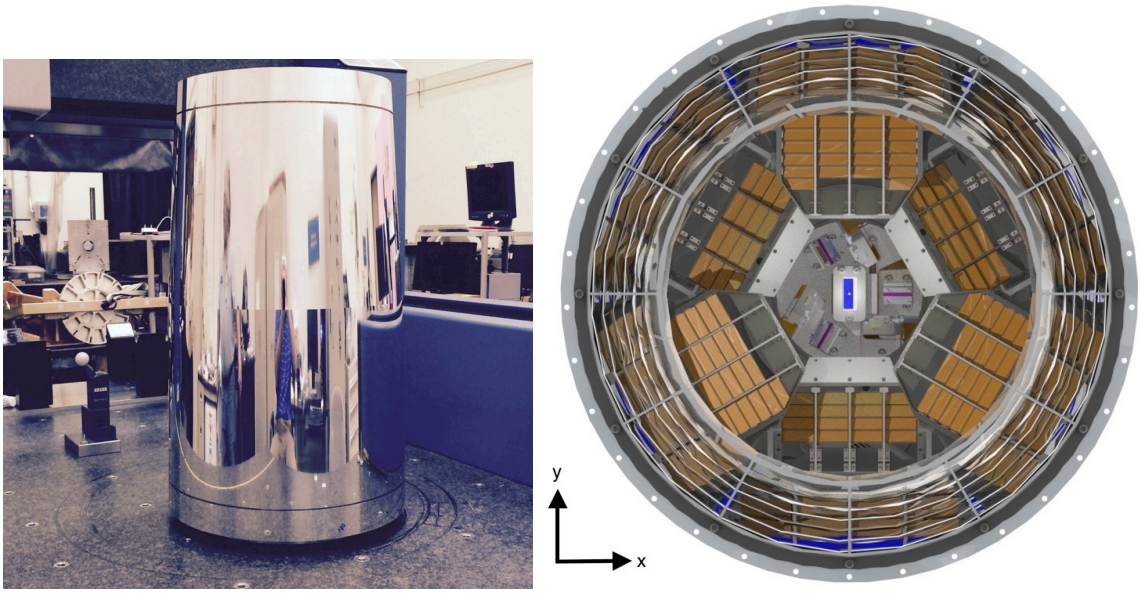

Figure 4: *Left:* A mirror mandrel made at MSFC, fabricated for the Micro-X project. The replication surface is 600 mm long. *Right:* View of the *REDSoX* Polarimeter front aperture, without the central baffling disk, vacuum box door, or focal plane baffle. Components are gratings (gold), LGMLs (magenta) and the direct imaging CCD (blue); the remaining CCDs are edge-on in this view. Gratings in the top and bottom sectors disperse to the right-most multilayer mirror, along the $+x$ axis.

an intricate process, the gratings are etched from Si wafers along crystal planes (see Fig. 5 for an example and a picture using SNL's scanning electron microscope). The sides of the bars are polished and the gratings are tilted upon mounting to enable reflection at less than the critical angle off of the sides. In this way, high efficiencies are achieved in +1 order as needed for *REDSoX*.

Over a dozen CAT gratings of 200 nm period and 4 μm membrane thickness have been tested in the MIT polarimetry beamline (§4), including several in a 28 mm square format fabricated as part of *Arcus* [55] phase A development. Fig. 5 shows a flight-like CAT grating mounted for testing in the polarimetry lab and a scanning electron microscope image of a small portion. We have shaken a grating along three axes to GEVS vibration levels and found no structural changes [26]. We used the beamline to verify the variation of the +1 efficiency with pitch angle (Fig. 6, Garner et al., in prep.) and determined that we will tilt them 0.8° to the incoming light to take advantage of blazing. Gratings will be aligned and glued into mounts before installing into subassemblies as seen in Fig. 7. Alignment is performed at the mount and subassembly level, as described in §3.5, using a method prototyped for *Arcus* [56].

The dispersion of each grating is given by the grating equation: $m\lambda = P \sin\phi$, where $P = 200$ nm is the grating period, m is the grating order of interest (which we take to be +1) and ϕ is the dispersion angle. Our goal is to match the dispersed wavelength to the peak reflectivity of the LGML, given by $\lambda = 2d\cos\theta$, where d is the multilayer period and θ is the angle of incidence relative to the LGML normal. For the LGML, $d = Gx$, where x is the distance along the LGML referenced to a location off of the LGML and $G = 0.88$Å/mm. Positioning details are given in

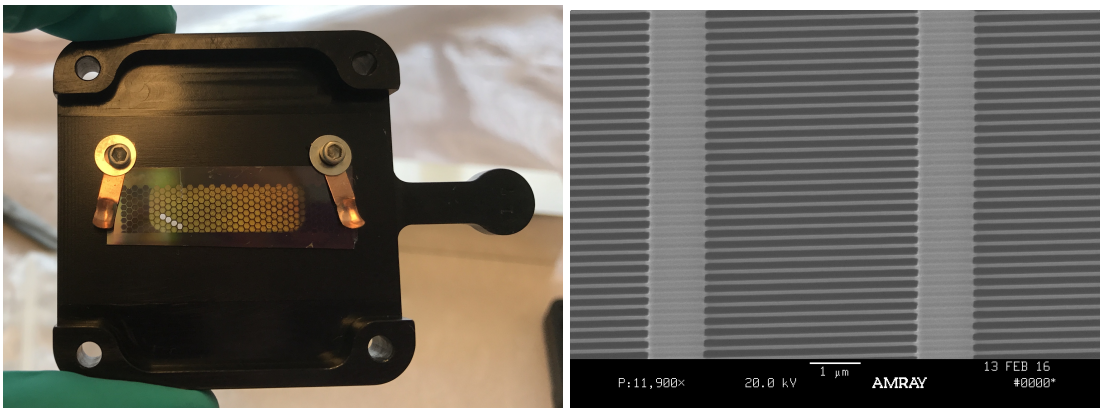

Figure 5: *Left:* A flight-like CAT grating, mounted for testing in the MIT Polarimetry Beamline. *Right:* Expanded view of a CAT grating. The 1 μm wide support structure has a 5 μm pitch and is 4 μm deep.

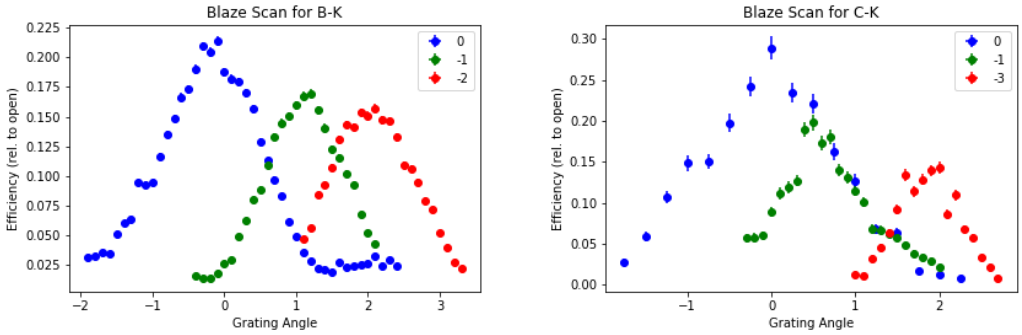

Figure 6: Absolute efficiency measurements of a flight-like grating at 0.183 keV (B-K, left) and 0.277 keV (C-K, right). The gratings were developed for *Arcus*, identical to those for *REDSoX* on a scale of a few mm, as measured here. The angle scans determine the blaze condition at which a given order (e.g. -1) has maximum dispersion efficiency. Measurements were obtained in the MIT Polarimetry Beamline (Garner et al., in prep.).

our paper [45] that includes raytrace validation. We solved for position along the optical axis as a function of azimuthal and radial location for each grating, resulting in a stairstepped grating subassembly, as illustrated in Fig. 7. In order to satisfy the Bragg condition at each of the LGMLs, the telescope attitude must be maintained along each of the three LGMLs to better than 7″ in 1D (1 σ), smaller than the optics PSF in 1D (§10). The attitude system chosen for our mission has been shown to be capable of maintaining control to 3″ in 1D along any given axis.

3.3 Laterally Graded Multilayer Mirrors (LGMLs)

Two LGMLs have been made by Eric Gullikson at the Lawrence Berkeley National Lab (LBNL) Center for X-ray Optics that are suitable for our design and only one more is needed, with an additional LGML as a spare. The Cr/B_4C/Sc layer combination has a reflectivity over 7% between 31 and 80 Å based on measurements at the Advanced Light Source at LBNL (Fig. 8) [43, 44]. We have tested a combination of LGMLs made by Reflective X-ray Optics that have comparable performance longward of the C-K and B-K edges at 45 and 67 Å, respectively [44].

Figure 7: An early design of the *REDSoX* grating module. Each grating in an upper subassembly disperses to the same LGML as those in the lower subassembly of the opposite sector. The gratings are stair-stepped to match the Bragg condition at the multilayer mirror (see §3.2 [45]).

While these would give 10-30% greater sensitivity, for *REDSoX* we choose the simple approach to use a single material combination and will consider other ML combinations for *REDSoX* upgrades (see §4.2).

3.4 CCD Detectors

We plan to use "off-the-shelf" commercial CCDs, which provides excellent cost value and allows us to take advantage of mature and well-tested software and readout electronics, at the expense of less flexibility on the form factor of the CCDs themselves. We plan to use three 2048x2048 CCD cameras from Raptor Photonics to record the dispersed, polarization-sensitive spectrum reflected by the LGMLs, and a fourth will record the zeroth-order source image to ensure proper acquisition of the target and monitor its broad-band flux, giving us a redundant measurement of Stokes I. The zeroth order detector will be defocused 15 mm to avoid physical interference with the LGMLs (see Fig. 9) and mitigate the effects of pileup.

The CCD spectral resolution requirements are modest, with FWHM < 200 eV required merely to reduce background and to distinguish 0.2 keV photons in 1st order from 0.4 keV in 2nd order in the dispersed spectra. We expect to operate at -50C to minimize dark current and CTI effects. Read noise for the baseline detectors is <3.5 e^- in their standard 75kHz readout mode (2.3 e^- typical), and <5 e^- when binning. A faster readout mode is available at 2MHz with typical read noise of 9.0 e^-, which can be useful in lab testing and for initial source acquisition in flight.

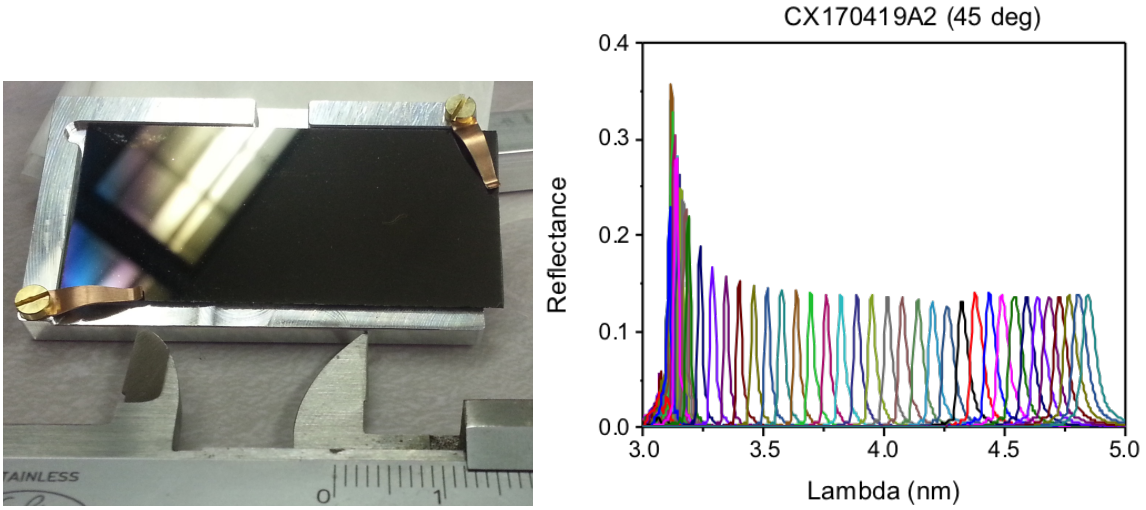

Figure 8: *Left:* A flight-like LGML in a test holder used in the MIT Polarimetry lab for testing. It is 0.5 mm thick and 47 mm long. The multilayer period increases from left to right. *Right:* Measurements of the LGML using a partially polarized beam at the Advanced Light Source [45]. The reflectivities were regularly sampled across the surface of the LGML. Reflectivities to unpolarized light average just over 7% over the 31-80 Å bandpass.

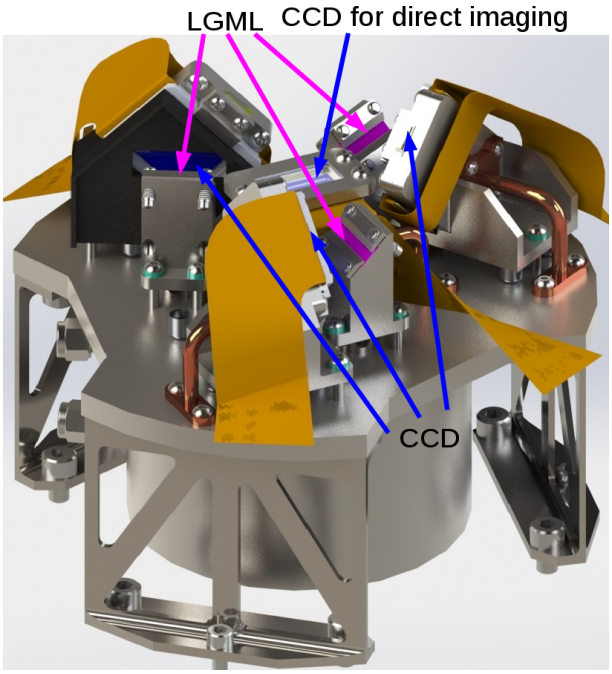

Figure 9: Preliminary design of the interior of the focal plane assembly showing the LGMLs and CCDs. The detectors are rotated 45° about their normal to lengthen the ranges of the spectra reflected by the LGMLs. This rendering is from an early focal plane design using e2v detectors connected via ribbon cables to headboards at the outside edge of the vacuum cylinder. Copper pieces connect the CCDs to the plate cooled with LN_2.

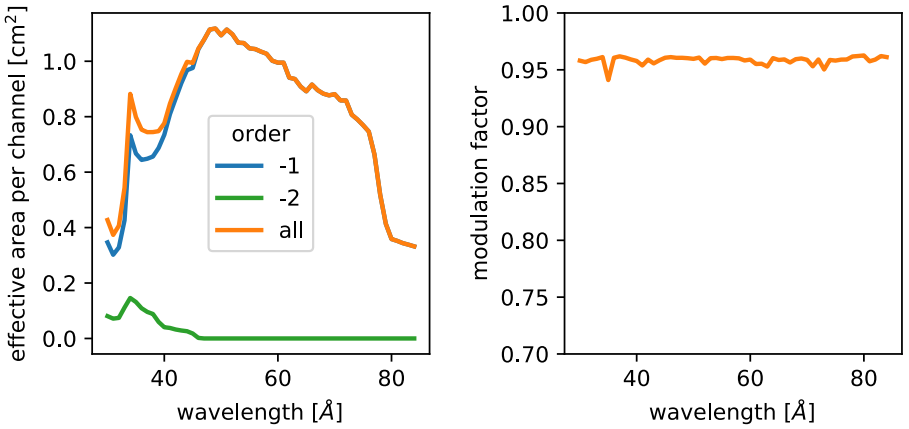

Figure 10: *Left:* Effective area per channel of the system based on raytracing [18, 45]. Second order contributes usefully for $\lambda < 40$Å. *Right:* The modulation factor is about 96% over the *REDSoX* band.

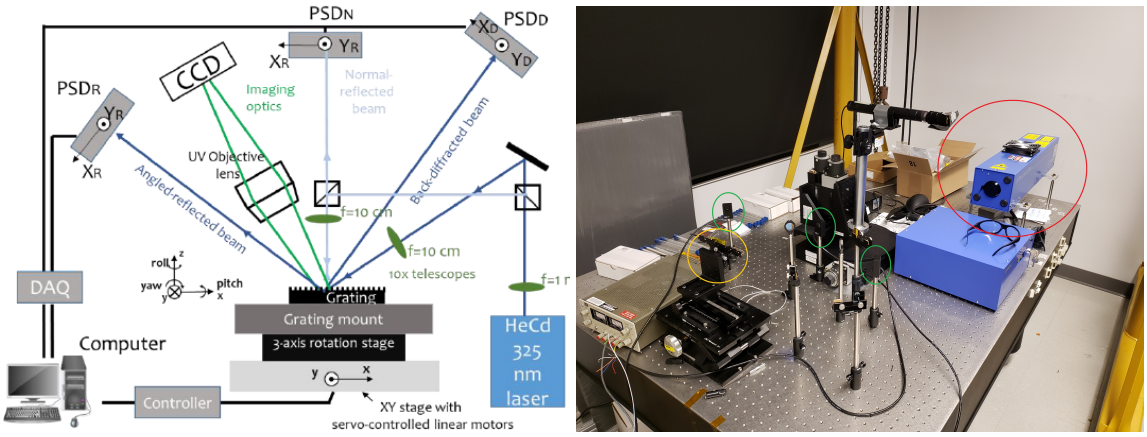

Figure 11: *Left:* Schematic of the laser reflection system for aligning *Arcus* CAT gratings [56]. *Right:* The same system setup for *REDSoX* but without the CCD camera. The UV alignment laser is circled in red. The setup uses three position-sensitive detectors (green) to characterize the orientation of the grating bars. It provides continuous feedback, which allows us to align the grating (yellow) using the adjustable grating mount (Fig. 5, right) [13].

3.5 Payload Assembly and Integration

Angular and positional tolerances were computed using raytrace simulations [18, 45] for each major component and for important individual parts. One important conclusion from raytracing is that the modulation factor (Fig. 10, right) does not vary significantly as components are shifted or rotated due to the small changes of the graze angles on the LGMLs [45].

Mirror shell alignment will take place at MSFC, using methods developed for *IXPE* and other missions. CAT grating alignment procedures have been developed and demonstrated as part of *Arcus* phase A work [24, 56] and with MIT internal funding [13]. The method is based on UV laser reflection and diffraction and was shown to be sufficient for *REDSoX*. We built such a grating alignment system, customized for *REDSoX* project (Fig. 11 [13]).

3.6 Sources of Background

From the Suzaku mission, the particle background in the backside-illuminated CCD (XIS1) was 1.5×10^{-4} cnt/s/DN/CCD at 0.3 keV (where DN is the digital number from the charge analog-to-

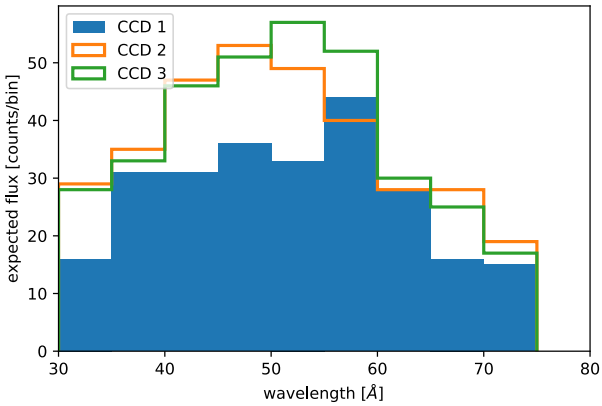

Figure 12: Sample result from raytracing a *REDSoX* observation of Mrk 421, assuming $P = 20\%$ in a direction perpendicular to channel 1's LGML. CCD 1 clearly shows fewer counts than the other two, demonstrating that a polarization of 20% can be detected.

digital converter [35]). With 4 eV/DN and a CCD area of about 608 mm^2, the *REDSoX* background is 1.5×10^{-5} cnt/s/mm^2 in a 0.2 keV band at 0.3 keV. Suzaku was in a low earth orbit, where the background should be less than that at the sounding rocket's apogee. Along the dispersion, the spectra are 50 mm long. Across the dispersion, the spectra consist of two bands, corresponding to either the upper or the lower gratings. Each band is about 0.5 mm wide due to divergence after reflection from the LGML; after including mirror blurring, the bands are about 0.9 mm across. Using three detectors and exposing for 300 s yields 1.2 counts expected from particles.

The X-ray background in the *REDSoX* bandpass is dominated by Galactic emission. A full ray-trace simulation including gratings and the LGMLs using the `marxs` code [17, 45] shows that off-axis X-rays are dispersed in such a way that their reflection is suppressed by the ML, in contrast to on-axis photons which are diffracted such that they hit the Bragg peak [18]. Using a measured flux for the Galactic emission and background AGN [2], the ray-trace predicts an X-ray background rate of 2 counts per 1 Ms. Compared to the source, at 500 counts, these backgrounds are negligible. A simulation is shown in Fig. 12, demonstrating how the *REDSoX* Polarimeter can be used to detect a polarization of 20%.

4. Project Status and Next Steps

The *REDSoX* project was approved by NASA and officially started in October 2022. Since then, we have set up our management team and started preparing for our preliminary design review (PDR). The optics group at MSFC started a design phase and preliminary mechanical analysis. Part of the work for the PDR involves prototyping gratings specifically for *REDSoX* and selecting a detector system; a CCD camera was obtained on loan from a potential vendor for X-ray testing in the MKI Polarimetry Beamline.

With MKI and APRA funding, we set up a beamline of polarized X-rays with spectral bandwidths of $< 0.02E$ for 0.17 keV $< E <$ 0.73 keV [26, 42, 49]. We will use the beamline to test CAT gratings for this project as we have done for *Arcus* (see Fig. 6) and measure the LGMLs before assembly and after mounting on the focal plane mounting plate. Once the LGMLs are mounted, the flight focal plane will be put on the detector chamber's X-Y stage for tests with a variety of polarized emission lines. Optics are not required for the focal plane alignment as a slit is used to collimate the X-ray beam to better than 3″, much smaller than the 1D PSF of the optics (see §3.1).

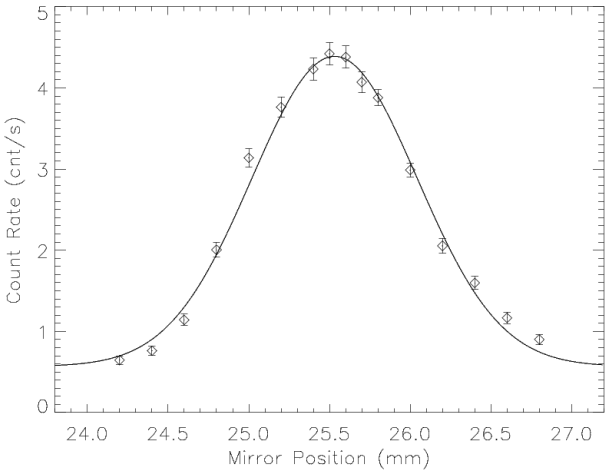

Figure 13: Result from testing a LGML using a carbon anode in the MIT polarimetry beamline. The LGML in the beamline can be moved laterally to select an energy for polarization, polarizing X-rays over a narrow energy band. The strong signal enables us to localize the optimum reflectivity to 12 μm [44].

The polarization angle of the X-ray source can be rotated so that the LGML modulation factor can be verified. We also have an optical bench for aligning gratings using a UV laser (Fig. 11).

4.1 Potential Upgrades to the *REDSoX* Polarimeter

The basic design of the *REDSoX* Polarimeter allows for several types of upgrades. These upgrades would extend the bandpass to higher energies and/or improve the MDP for a given source. Examples of upgrades are 1) taller CAT gratings with increased efficiencies [25], 2) adding mirror shells to increase the effective area, 3) using existing higher efficiency LGMLs for longer wavelengths to improve sensitivity below 0.28 keV [44], 4) using LGMLs designed to reflect at 30° graze angles to increase the band beyond 0.4 keV up to 0.8 keV, 5) and potentially using twisted crystals to work up to 1 keV [12]. For example, the efficiency of the CAT grating improves by 20-30% if these structures are 6 μm tall. The grating group at MIT is already working to increase the grating height with funding for *Arcus* prototyping. With such gratings, the system MDP would drop by 15%, so an MDP of 60% would improve to 50%. Work on 30° LGMLs and twisted crystals are currently funded by APRA.

4.2 Potential Orbiting Soft X-ray Polarimeters

An instrument of *REDSoX* design has substantially more potential as a baseline design for future soft X-ray polarimetry than designs based on ML-coated primary optics like LAMP [54] or concentrators with ML-coated reflectors [50]. LAMP, for example, would have an integrated reflectivity to unpolarized light of 0.5 eV over a 5 eV band [54], while our design has an integrated reflectivity of 4 eV over a 200 eV band. Our design makes ×8 better use of a given optics effective area and exposure time as well as providing spectroscopy over a ×40 wider band. More importantly, the scientific advantage of our approach is evident in Fig. 3 (center), which shows that one can detect a polarized spectral feature with a relatively small signal using a spectropolarimeter designed like *REDSoX*.

The *REDSoX* Polarimeter design is suitable for a NASA Mission of Opportunity for small satellites. An instrument in low Earth orbit such as the Globe Orbiting Soft X-ray Polarimeter (*GOSoX*), proposed in response to a NASA Astrophysics Pioneers call, could integrate much longer

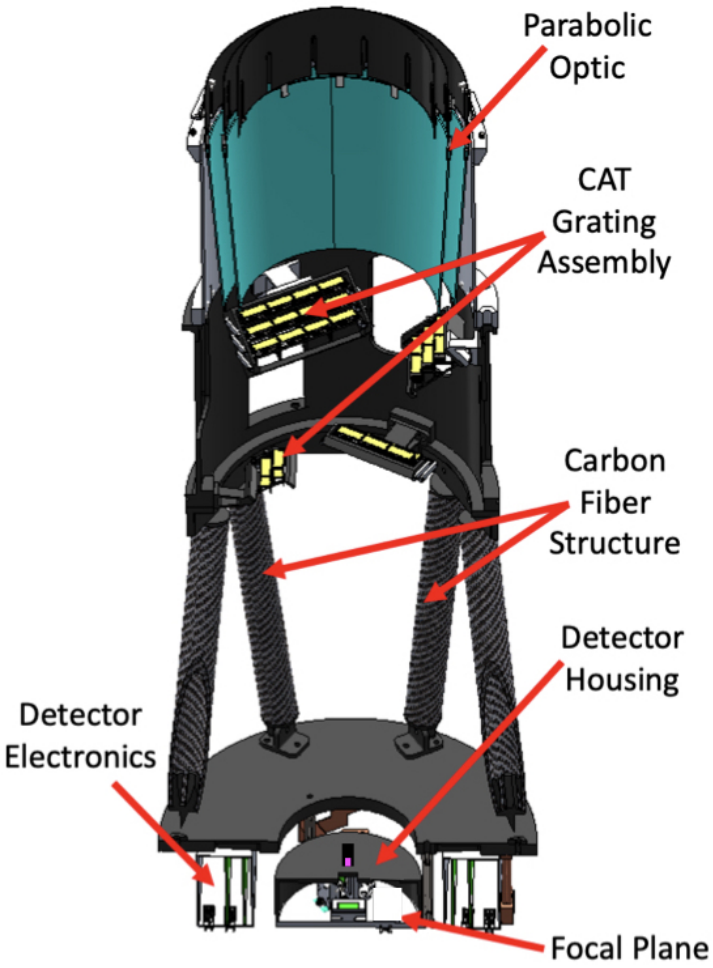

Figure 14: Cutaway rendering of the configuration of a soft X-ray polarimeter proposed for the *GOSoX* mission [46]. Optics are shown in cyan, gratings are shown in yellow, the detectors are shown in green and the LGMLs are shown in purple. Some structural components have been hidden in this view to improve the visibility of the optical components. It is about 1.25 m tall. The orientations of the grating bars are parallel to their short dimensions and blazed so that opposite sectors ("high" and "low") disperse to a common LGML inside the detector housing. As with *REDSoX*, there would be three polarimetry channels. The design is functionally identical to *REDSoX* except that it is ×2 shorter, has only two parabolic mirror shells, and has detectors that are cooled thermoelectrically.

[46]. A rendering of the instrument is shown in Fig. 14. In 200ks, *GOSoX* would achieve an MDP of 1.9% for Mrk 421 with the same components as we propose for *REDSoX* but with a smaller mirror effective area. Polarization variability studies of blazars are almost routine optically [32] and would be feasible in soft X-rays for blazars and tidal disruption events. For an isolated neutron star such as RX J0720−3125, the MDP would be <5% in a week-long observation, allowing for phase- or energy-resolved polarimetry. Spectropolarimetry with *GOSoX* could be used to test the nature of absorption features in the atmospheres of neutron stars and examine the reflected continuum between emission lines in Sy 2 galaxies. Such an instrument would complement any high energy photoelectron-tracking polarimeter such as *IXPE*. Launching the *REDSoX* Polarimeter would raise the TRLs of all of the components needed for *GOSoX*.

Only our soft X-ray polarimeter design can share optics necessary for higher energy instruments. Thus, our soft X-ray polarimeter could be combined with polarimeters working at higher energies such as on the X-ray Polarimetry Probe (XPP, [34]). XPP would have a focusing mirror with CAT gratings to disperse soft X-rays to LGMLs and CCD detectors for the soft channel. The gratings are practically transparent to X-rays above 2 keV, so higher energy X-rays pass through the gratings to a time projection chamber (TPC) polarimeter like that proposed for PRAXyS [33] to measure X-ray polarization in the 2-10 keV range. Furthermore, the TPC can be constructed with an exit window to allow high energy X-rays to pass to LiH/scintillator scattering rods surrounded by Cd-

Zn-Te detectors to measure polarizations up to 50 keV (based on X-Calibur, [1, 3]). This way, three polarimeters can share a large focusing optic, providing polarization measurements over the 0.2-50 keV band simultaneously. XPP could also have a telescope dedicated to an imaging X-ray polarimeter, using detectors like those developed for *IXPE*.

Acknowledgments

Funding for this work was provided in part by grant 80NSSC23K0644 from NASA in support of the *REDSoX* Polarimeter, a NASA Astrophysics sounding rocket mission. Support for this work was also provided in part by the National Aeronautics and Space Administration (NASA) through the Smithsonian Astrophysical Observatory (SAO) contract SV3-73016 to MIT for support of the Chandra X-Ray Center (CXC), which is operated by SAO for and on behalf of NASA under contract NAS8-03060.

References

[1] Abarr, Q., Awaki, H., Baring, M. G., et al. 2021, Astroparticle Physics, 126, 102529, doi: 10.1016/j.astropartphys.2020.102529

[2] Bautz, M. W., Miller, E. D., Sanders, J. S., et al. 2009, PASJ, , 61, 1117, doi: 10.1093/pasj/61.5.1117

[3] Beilicke, M., Kislat, F., Zajczyk, A., et al. 2014, Journal of Astronomical Instrumentation, 3, 1440008, doi: 10.1142/S225117171440008X

[4] Bogdanov, S., Guillot, S., Ray, P. S., et al. 2019, ApJ, , 887, L25, doi: 10.3847/2041-8213/ab53eb

[5] Bogdanov, S., Lamb, F. K., Mahmoodifar, S., et al. 2019, ApJ, , 887, L26, doi: 10.3847/2041-8213/ab5968

[6] Borghese, A., Rea, N., Coti Zelati, F., et al. 2017, MNRAS, , 468, 2975, doi: 10.1093/mnras/stx632

[7] Cash, W. 1987, Appl.Optics, , 26, 2915, doi: 10.1364/AO.26.002915

[8] Cottam, J., Paerels, F., & Mendez, M. 2002, Nature, , 420, 51, doi: 10.1038/nature01159

[9] Cottam, J., Paerels, F., Méndez, M., et al. 2008, ApJ, , 672, 504, doi: 10.1086/524186

[10] Di Gesu, L., Marshall, H. L., Ehlert, S. R., et al. 2023, Nature Astronomy, doi: 10.1038/s41550-023-02032-7

[11] Donato, D., Ghisellini, G., Tagliaferri, G., & Fossati, G. 2001, A&A, , 375, 739, doi: 10.1051/0004-6361:20010675

[12] Garner, A., Marshall, H., Heine, S., et al. 2019, in SPIE Conference Series, , Vol. 11118, Society of Photo-Optical Instrumentation Engineers (SPIE) Conference Series, 1111811–1–12

[13] Garner, A., Marshall, H. L., Trowbridge Heine, S. N., et al. 2020, in Society of Photo-Optical Instrumentation Engineers (SPIE) Conference Series, Vol. 11444, Society of Photo-Optical Instrumentation Engineers (SPIE) Conference Series, 114445Z, doi: 10.1117/12.2561734

[14] Gianolli, V. E., Kim, D. E., Bianchi, S., et al. 2023, MNRAS, , 523, 4468, doi: 10.1093/mnras/stad1697

[15] Ginzburg, V. L., & Syrovatskii, S. I. 1965, ARA&A, , 3, 297, doi: 10.1146/annurev.aa.03.090165.001501

[16] Gubarev, M., Ramsey, B., Kolodziejczak, J. J., et al. 2014, in SPIE Conference Series, , Vol. 9144, Space Telescopes and Instrumentation 2014: Ultraviolet to Gamma Ray, 91444U, doi: 10.1117/12.2056595

[17] Günther, H. M., Frost, J., & Theriault-Shay, A. 2017, AJ, , 154, 243, doi: 10.3847/1538-3881/aa943b

[18] Günther, H. M., Marshall, H. L., & Garner, A. 2020, in Society of Photo-Optical Instrumentation Engineers (SPIE) Conference Series, Vol. 11444, Space Telescopes and Instrumentation 2020: Ultraviolet to Gamma Ray, ed. J.-W. A. den Herder, S. Nikzad, & K. Nakazawa, 1144460, doi: 10.1117/12.2562860

[19] Haberl, F. 2007, Ap&SS, , 308, 181, doi: 10.1007/s10509-007-9342-x

[20] Haberl, F., Zavlin, V. E., Trümper, J., & Burwitz, V. 2004, A&A, , 419, 1077, doi: 10.1051/0004-6361:20034129

[21] Harding, A. K., & Lai, D. 2006, Reports on Progress in Physics, 69, 2631, doi: 10.1088/0034-4885/69/9/R03

[22] Heilmann, R. K., Bruccoleri, A. R., & Schattenburg, M. L. 2015, in SPIE Conference Series, , Vol. 9603, Society of Photo-Optical Instrumentation Engineers (SPIE) Conference Series, 960314, doi: 10.1117/12.2188525

[23] Heilmann, R. K., Ahn, M., Bautz, M. W., et al. 2009, in SPIE Conference Series, , Vol. 7437, Optics for EUV, X-Ray, and Gamma-Ray Astronomy IV, 74370G, doi: 10.1117/12.825394

[24] Heilmann, R. K., Bruccoleri, A. R., Song, J., et al. 2017, in Society of Photo-Optical Instrumentation Engineers (SPIE) Conference Series, Vol. 10399, Society of Photo-Optical Instrumentation Engineers (SPIE) Conference Series, 1039914, doi: 10.1117/12.2273000

[25] Heilmann, R. K., Bruccoleri, A. R., Song, J., et al. 2021, in Society of Photo-Optical Instrumentation Engineers (SPIE) Conference Series, Vol. 11822, Society of Photo-Optical Instrumentation Engineers (SPIE) Conference Series, 1182215, doi: 10.1117/12.2594951

[26] Heine, S. N. T., Marshall, H. L., Heilmann, R. K., et al. 2017, in Society of Photo-Optical Instrumentation Engineers (SPIE) Conference Series, Vol. 10399, Society of Photo-Optical Instrumentation Engineers (SPIE) Conference Series, 1039916, doi: 10.1117/12.2274205

[27] Heyl, J. S., & Shaviv, N. J. 2002, PhysRevD, , 66, 023002

[28] Heyl, J. S., Shaviv, N. J., & Lloyd, D. 2003, Monthly Notices of the Royal Astronomical Society, 342, 134, doi: 10.1046/j.1365-8711.2003.06521.x

[29] Hickox, R. C., & Vrtilek, S. D. 2005, ApJ, , 633, 1064, doi: 10.1086/491596

[30] Ho, W. C. G., & Mori, K. 2008, in American Institute of Physics Conference Series, Vol. 983, 40 Years of Pulsars: Millisecond Pulsars, Magnetars and More, ed. C. Bassa, Z. Wang, A. Cumming, & V. M. Kaspi, 340–344, doi: 10.1063/1.2900178

[31] Hohle, M. M., Haberl, F., Vink, J., de Vries, C. P., & Neuhäuser, R. 2012, MNRAS, , 419, 1525, doi: 10.1111/j.1365-2966.2011.19809.x

[32] Hovatta, T., & Lindfors, E. 2019, New Astr. Rev., 87, 101541, doi: 10.1016/j.newar.2020.101541

[33] Jahoda, K., Kallman, T. R., Kouveliotou, C., et al. 2016, in SPIE Conference Series, , Vol. 9905, Society of Photo-Optical Instrumentation Engineers (SPIE) Conference Series, 990516, doi: 10.1117/12.2234220

[34] Jahoda, K., Krawczynski, H., Kislat, F., et al. 2019, arXiv e-prints, arXiv:1907.10190. https://arxiv.org/abs/1907.10190

[35] LaMarr, B., Grant, C., Kissel, S., et al. 2008, in SPIE Conference Series, , Vol. 7011, Space Telescopes and Instrumentation 2008: Ultraviolet to Gamma Ray, 70112C, doi: 10.1117/12.788168

[36] Liodakis, I., Marscher, A. P., Agudo, I., et al. 2022, arXiv e-prints, arXiv:2209.06227. https://arxiv.org/abs/2209.06227

[37] Marin, F., Goosmann, R. W., Dovčiak, M., et al. 2012, MNRAS, , 426, L101, doi: 10.1111/j.1745-3933.2012.01335.x

[38] Markoff, S., Falcke, H., & Fender, R. 2001, A&A, , 372, L25, doi: 10.1051/0004-6361:20010420

[39] Marscher, A. P. 2014, ApJ, , 780, 87, doi: 10.1088/0004-637X/780/1/87

[40] Marshall, H. L. 2007, in SPIE Conference Series, , Vol. 6688, Optics for EUV, X-Ray, and Gamma-Ray Astronomy III. Edited by O'Dell, Stephen L.; Pareschi, Giovanni. Proceedings of the SPIE, Volume 6688, pp. 66880Z (2007)., doi: 10.1117/12.746957

[41] Marshall, H. L., Murray, S. S., Chappell, J. H., et al. 2003, in SPIE Conference Series, , Vol. 4843, Polarimetry in Astronomy. Edited by Silvano Fineschi . Proceedings of the SPIE, Volume 4843, pp. 360-371 (2003)., ed. S. Fineschi, 360–371

[42] Marshall, H. L., Schulz, N. S., Remlinger, B., et al. 2013, in SPIE Conference Series, , Vol. 8861, Society of Photo-Optical Instrumentation Engineers (SPIE) Conference Series, doi: 10.1117/12.2025727

[43] Marshall, H. L., Schulz, N. S., Windt, D. L., et al. 2014, in SPIE Conference Series, , Vol. 9144, Society of Photo-Optical Instrumentation Engineers (SPIE) Conference Series, 1, doi: 10.1117/12.2057003

[44] Marshall, H. L., Schulz, N. S., Windt, D. L., et al. 2015, in SPIE Conference Series, , Vol. 9603, Society of Photo-Optical Instrumentation Engineers (SPIE) Conference Series, 960319, doi: 10.1117/12.2188452

[45] Marshall, H. L., Günther, H. M., Heilmann, R. K., et al. 2018, Journal of Astronomical Telescopes, Instruments, and Systems, 4, 11004, doi: 10.1117/1.JATIS.4.1.011004

[46] Marshall, H. L., Heine, S. N. T., Davidson, R., et al. 2021, in Society of Photo-Optical Instrumentation Engineers (SPIE) Conference Series, Vol. 11822, Society of Photo-Optical Instrumentation Engineers (SPIE) Conference Series, 118220O, doi: 10.1117/12.2596186

[47] McClintock, J. E., Haswell, C. A., Garcia, M. R., et al. 2001, ApJ, , 555, 477, doi: 10.1086/321449

[48] McNamara, A. L., Kuncic, Z., & Wu, K. 2009, MNRAS, , 395, 1507, doi: 10.1111/j.1365-2966.2009.14608.x

[49] Murphy, K. D., Marshall, H. L., Schulz, N. S., et al. 2010, in SPIE Conference Series, , Vol. 7732, Society of Photo-Optical Instrumentation Engineers (SPIE) Conference Series

[50] Panini, S., Sreekumar, P., Marshall, H. L., et al. 2017, Journal of Astronomical Telescopes, Instruments, and Systems, 4, 11002, doi: 10.1117/1.JATIS.4.1.011002

[51] Potekhin, A. Y., Suleimanov, V. F., van Adelsberg, M., & Werner, K. 2012, A&A, , 546, A121, doi: 10.1051/0004-6361/201219747

[52] Ramsey, B. D., Elsner, R. F., Engelhaupt, D., et al. 2004, in SPIE Conference Series, , Vol. 5168, Optics for EUV, X-Ray, and Gamma-Ray Astronomy, ed. O. Citterio & S. L. O'Dell, 129–135, doi: 10.1117/12.509619

[53] Schnittman, J. D., & Krolik, J. H. 2009, ApJ, , 701, 1175, doi: 10.1088/0004-637X/701/2/1175

[54] She, R., Feng, H., Muleri, F., et al. 2015, in SPIE Conference Series, , Vol. 9601, UV, X-Ray, and Gamma-Ray Space Instrumentation for Astronomy XIX, 96010I, doi: 10.1117/12.2186133

[55] Smith, R. K., Abraham, M., Allured, R., et al. 2017, in Society of Photo-Optical Instrumentation Engineers (SPIE) Conference Series, Vol. 10397, Society of Photo-Optical Instrumentation Engineers (SPIE) Conference Series, 103970Q, doi: 10.1117/12.2272818

[56] Song, J., Heilmann, R. K., Bruccoleri, A. R., Hertz, E., & Schatternburg, M. L. 2017, in Society of Photo-Optical Instrumentation Engineers (SPIE) Conference Series, Vol. 10399, Society of Photo-Optical Instrumentation Engineers (SPIE) Conference Series, 1039915, doi: 10.1117/12.2274206

[57] Suleimanov, V., Hambaryan, V., Potekhin, A. Y., et al. 2010, A&A, , 522, A111, doi: 10.1051/0004-6361/200913641

[58] Suleimanov, V., Potekhin, A. Y., & Werner, K. 2009, A&A, , 500, 891, doi: 10.1051/0004-6361/200912121

[59] Tavecchio, F., Landoni, M., Sironi, L., & Coppi, P. 2018, MNRAS, , 480, 2872, doi: 10.1093/mnras/sty1491

[60] Taverna, R., Turolla, R., Gonzalez Caniulef, D., et al. 2015, MNRAS, , 454, 3254, doi: 10.1093/mnras/stv2168

[61] Ursini, F., Marinucci, A., Matt, G., et al. 2023, MNRAS, , 519, 50, doi: 10.1093/mnras/stac3189

[62] Vieyro, F. L., Romero, G. E., & Chaty, S. 2016, A&A, , 587, A63, doi: 10.1051/0004-6361/201526587

[63] Weisskopf, M. C., Cohen, G. G., Kestenbaum, H. L., et al. 1976, ApJ, , 208, L125, doi: 10.1086/182247

[64] Weisskopf, M. C., Ramsey, B., O'Dell, S., et al. 2016, in SPIE Conference Series, , Vol. 9905, Society of Photo-Optical Instrumentation Engineers (SPIE) Conference Series, 990517, doi: 10.1117/12.2235240

[65] Weisskopf, M. C., Soffitta, P., Baldini, L., et al. 2022, Journal of Astronomical Telescopes, Instruments, and Systems, 8, 026002, doi: 10.1117/1.JATIS.8.2.026002

[66] Zhuravlev, A., Taverna, R., & Turolla, R. 2022, ApJ, , 925, 80, doi: 10.3847/1538-4357/ac397e

PoS(MULTIF2023)076